

Assessing the Suitability of Cellulose-Nanodiamond Composite As a Multifunctional Biointerface Material for Bone Tissue Regeneration

Karlene Vega-Figueroa,^{†,‡,||} Jaime Santillán,^{†,§,||} Carlos García,^{†,‡,||} José A. González-Feliciano,^{||} Samir A. Bello,[‡] Yaiel G. Rodríguez,^{‡,||} Edwin Ortiz-Quiles,^{‡,||} and Eduardo Nicolau^{*,‡,||}

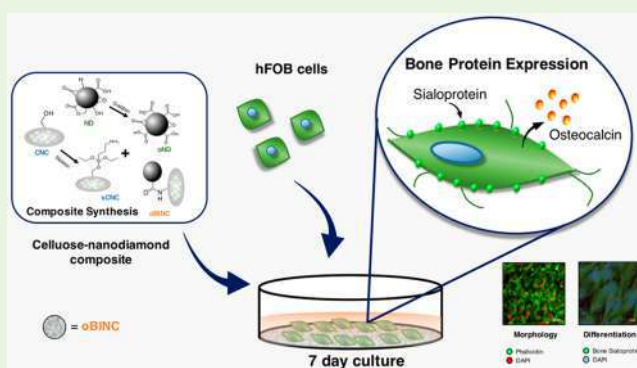
[†]Department of Biology, [§]Department of Physics, and [‡]Department of Chemistry, University of Puerto Rico, Rio Piedras Campus, San Juan, Puerto Rico 00931-3346, United States

^{||}Molecular Science Research Center, University of Puerto Rico, 1390 Ponce De León Avenue, Suite 2, San Juan, Puerto Rico 00926, United States

S Supporting Information

ABSTRACT: Interfacial surface properties, both physical and chemical, are known to play a critical role in achieving long-term stability of cell–biomaterial interactions. Novel bone tissue engineering technologies, which provide a suitable interface between cells and biomaterials and mitigate aseptic osteolysis, are sought and can be developed via the incorporation of nanostructured materials. In this sense, engineered nanobased constructs provide an effective interface and suitable topography for direct interaction with cells, promoting faster osseointegration and anchoring. Therefore, herein we have investigated the surface functionalization, biocompatibility, and effect of cellulose-nanodiamond conjugates on osteoblast proliferation and differentiation. Cellulose nanocrystals (CNC) were aminated through a 3-aminopropyltriethoxysilane (APTES) silylation, while nanodiamonds (ND) were treated with a strong acid oxidation reflux, as to produce carboxyl groups on the surface. Thereafter, the two products were covalently joined through an amide linkage, using a common bioconjugation reaction. Human fetal osteoblastic cells (hFOB) were seeded for 7 days to investigate the in vitro performance of the cellulose-nanodiamond conjugates. By employing immunocytochemistry, the bone matrix expression of osteocalcin (OC) and bone sialoprotein (BSP) was analyzed, demonstrating the viability and capacity of osteoblasts to proliferate and differentiate on the developed composite. These results suggest that cellulose-nanodiamond composites, which we call oxidized biocompatible interfacial nanocomposites (oBINC), have the potential to serve as a biointerface material for cell adhesion, proliferation and differentiation because of their osteoconductive properties and biocompatibility; furthermore, they show promising applications for bone tissue regeneration.

KEYWORDS: nanocellulose, nanodiamonds, bone regeneration, biofabrication, biointerface materials, biomedical applications



1. INTRODUCTION

Cell–biomaterial interfaces are crucial in regulating cell fate via complex interplay between chemical and physical signals. Studies demonstrate that the surface properties of these biomaterials can be engineered to create unique and suitable microenvironments to the extent that cellular interactions are altered accordingly.¹ Specifically, increasing the surface area and changing surface functional groups are strategies employed to better enhance these cell–material interactions.^{2,3} It is of particular consideration that the tuned and applied modifications should be aimed in mimicking the cells' extracellular matrix structure, a crucial property for proper adhesion and proliferation.^{4–7} In this sense, nanostructured materials have been shown to provide interesting surface topographies given that its properties may be refined to produce different forms of stimulation (e.g., mechanical, chemical, or electrical), which in

turn may guide cells in further development.^{6,8,9} On the basis of this understanding, we have evaluated the use of nanocellulose (CNC) composites conjugated with nanodiamonds (ND) as a promising biointerface material that provides structural support, as well as stimulation for cell proliferation, differentiation and migration of human fetal osteoblasts (hFOB).

Natural polymers such as cellulose have been shown to be noncytotoxic and chemically versatile due to the abundance of surface hydroxyl groups, which allows for further modifications of its intrinsic properties.^{10–13} Even more so, studies have demonstrated that the piezoelectricity of cellulose may provide positive, electrical stimulus to cells, which in all could provide

Received: January 11, 2017

Accepted: April 2, 2017

Published: April 3, 2017

further capabilities to the proposed biocompatible interfacial material.^{14–17} Nonetheless, it is CNC's rigidity that makes it a structurally outstanding compound with a Young's modulus of 167.5 GPa, comparable to that of titanium.¹⁸ Such characteristics have made cellulose a promising biomaterial for bone tissue engineering applications (BTE). Yet, it must be noted that cellulose by itself does not possess active healing properties. As a means to mitigate such demerit, the incorporation of nanoparticles, such as nanodiamonds, would allow for the design of a more bioactive interface material.

On the other hand, nanodiamonds not only exhibit various intriguing characteristics such as chemical stability, stiffness, and strength, but also their small size and high surface area pertain advantageous qualities as nanoparticles. Much of their proven versatility is due to the presence of sp^2 carbons, which allow for chemical modifications such as the addition of carboxylic acids.^{19–21} Moreover, tailoring molecules with carboxyl group moieties on their surface has proven to facilitate extracellular protein interactions that result in cell adhesion.³ Therefore, NDs may provide superior physical and chemical properties over conventional materials.

In the present study, cellulose-nanodiamond conjugates were synthesized using detonation nanodiamonds and cellulose nanocrystals as precursor materials. The first step consisted in the chemical functionalization of ND and CNC, via an oxidative acid reflux reaction and APTES silylation, respectively. Subsequently, the products obtained through these reactions were joined by means of EDC/Sulfo-NHS covalent coupling. In order to investigate the *in vitro* proliferation and differentiation of human fetal osteoblastic cells (hFOB), cellulose-nanodiamond analogues were assessed for their nanostructured suitability and chemical compatibility as a material interface for cell growth. Immunocytochemical and morphological studies were performed to evaluate cytotoxicity and protein expression as positive indicators for cell maturation for osteoblast cultured on the covalently linked nanomaterials: CNC, silylated cellulose nanocrystals (sCNC), nanodiamonds (ND), and oxidized nanodiamonds (oND).

2. MATERIALS AND METHODS

2.1. Materials. All reagents throughout the entire work were used as-received and without further purification. An 11.8% aqueous solution of cellulose nanocrystals was purchased from The Process Development Center (University of Maine, Orono, ME, USA). Ultra-Dispersed nonoxidized nanodiamonds (ND) were purchased from NanoGroup, Co. (Prague, CZ). 3-aminopropyltriethoxysilane (APTES), concentrated Sulfuric acid (H_2SO_4) and Nitric acid (HNO_3) were purchased from Sigma-Aldrich (USA). Nanopure water was obtained from a Milli-Q Direct 16 water purification system (18.2 M Ω /cm Millipore, USA) and was used for all the experiments.

2.2. Cellulose Silylation. To add an amine group to the primary hydroxyl group of CNC, we mixed 15 mL CNC (3% w/v) and 15 mL of APTES 0.1 M in an ethanol/water solvent (80:20). This mixture was stirred magnetically at 60 °C for 2 h. The resulting silylated cellulose nanocrystals were filtered several times with water to remove excess APTES.²²

2.3. Diamond Oxidation. A strong acid oxidation was employed to add carboxyl groups to the surface of the ND. To achieve this, 1 g of ND, 90 mL of concentrated H_2SO_4 , and 10 mL of concentrated HNO_3 were refluxed for 72 h. Then, the product of the reflux was filtered with water until an approximate pH of 7 was reached. The resulting oxidized nanodiamonds were dried at 105 °C in an oven overnight.^{23,24}

2.4. Composite Synthesis. The sCNC amine and oND carboxyl were linked covalently through an EDC (1-ethyl-3-(3-

(dimethylamino)propyl) carbodiimide) reaction. First, 100 mg of oND, 1 g EDC (Sigma-Aldrich, USA), 200 mg of sulfo-NHS (N-hydroxysulfosuccinimide) (Sigma-Aldrich, USA) and 45 mL of phosphate buffered solution 1X, pH 7.2 (PBS) (ThermoFischer Scientific, USA) were added and stirred magnetically for 15 min in a beaker at room temperature. Afterward, 10 mL of sCNC were added to the beaker and stirred for another 2 h. The produced oxidized biocompatible interfacial nanocomposite (oBINC) was purified in three ways. The crude of the reaction was dialyzed in a 15 kDa dialysis membrane (Spectrum Laboratories, Inc., USA) in 1 L of water for 24 h. Then, it was centrifuged (Sorvali Lynx 4000 Centrifuge, Thermo Scientific) four times at 10 000 rpm for 10 min. The supernatant was discarded after each centrifugation and the precipitate was resuspended with nanopure water. Lastly, the product was lyophilized and filtered with 50% ethanol. These reaction and purification steps were also done with untreated ND to provide a comparison to study the effectiveness of the process.^{25,26}

2.5. Composite Characterization. The construct (oBINC) and its control group analogue, biocompatible interfacial nanocomposite (BINC) were characterized using instrumental techniques to verify the effectiveness of the ND oxidation, the EDC linkage, surface area and stability. Reflectance FTIR (Nicolet Continuum FT-IR Microscope, Thermo Scientific) and Raman (780 nm LASER DXR Raman Microscope, Thermo Scientific) spectra were used to study the bonds and functional groups present in the product. Thermal gravimetric analysis (TGA) (Simultaneous Thermal Analyzer, STA 6000, PerkinElmer) assessed the thermal stability of the product from 30 to 950 °C under air flow at a rate of 20.00 °C/min. The surface area of the ND analogues was also studied using a Tristar 3020 after degassing at 110 °C under nitrogen flow for 8 h. High-resolution analysis of X-ray photoelectron spectroscopy (XPS) was conducted in order to ascertain the peptide bond formation between the sCNC and oND. X-ray Photoelectron spectroscopy (XPS) binding energy were obtained using a PHI 5600 spectrometer equipped with an Al K α mono and polychromatic X-ray source operating at 15 kV, 350 W and pass energy of 58.70 eV. All the binding energies reported were corrected using the carbon 1s peak (C 1s) at 284.8 eV. Deconvolution of the high-resolution results were completed using MultiPak (version 9.4.0.7) data reduction software.

2.6. Cell Line. Human fetal osteoblasts (cell line hFOB 1.19) from the American Type Culture Collection (Manassas, VA, USA) were used to test the biocompatibility of the conjugates described above. hFOB 1.19 cells were grown in 75 cm² plastic culture flasks (Corning, USA) and incubated at 34 °C with 5% CO₂ in a 1:1 mixture of Ham's F12 Medium/Dulbecco's Modified Eagle's Medium supplemented with 2.5 mM L-glutamine, 10% fetal bovine serum, and 0.3 mg/mL G418. When cells from passages 3–5 reached subconfluence, they were washed with phosphate buffered saline, harvested using 0.25% trypsin at 37 °C for 5 min, counted with an automated cell counter (BioRad), and used for the biocompatibility studies. All the reagents for cell culture were purchased to Thermo Fisher Scientific, USA.

2.7. Biocompatibility Studies. We evaluated the biocompatibility of the covalently linked cellulose nanocrystals and nanodiamonds by determining their effects on hFOB 1.19 cell morphology, adhesion and differentiation when used as cell culture substrates.

2.7.1. Nanoparticle Effects on hFOB Morphology and Adhesion. Initially, CNC, sCNC, oND, ND, oBINC, and BINC materials were suspended in 70% ethanol in a concentration of 1 mg/mL. Subsequently, 70 μ L of each material in suspension were deposited on 12 mm diameter glass coverslips (Neuvitro, USA) placed in 24-well plates (Ultralow attachment surface plates, Corning, USA). The ethanol was allowed to evaporate overnight and the entire plate was sterilized with UV light. After a rinse with PBS, 5×10^4 hFOB 1.19 cells were seeded on each coverslip and incubated for 7 days at 34 °C and 5% CO₂. Osteoblasts seeded on uncoated glass coverslips were used as controls. Medium was renewed every 2 days. After incubation, cells were fixed with 4% paraformaldehyde in PBS (Electron Microscopy Sciences, USA) for 1 h at room temperature. After two rinses with PBS, they were permeabilized with 0.1% Triton X-100 (Sigma-Aldrich, USA) for 15 min at room temperature. Cells were

washed twice with PBS, for 5 min each wash. Next, cells were incubated with FITC-conjugated Phalloidin (1:100, Sigma) for an hour at room temperature in the dark. After washing three times with PBS, samples were mounted in 24 × 60 mm coverslips with ProLong Diamond Antifade reagent (Molecular probes) containing 4',6-diamidino-2-phenylindole (DAPI) and stored at room temperature in the dark. Finally, samples were observed using a Nikon Eclipse Ni fluorescence microscope. Photographs of the cells (FITC-Phalloidin staining) or cell nuclei (DAPI staining) observed on the different substrates were taken using the Nikon DS-Q12 digital camera. The number of nuclei per visual field (20X, 0.35 mm²) was counted on photographs using the cell counter plugin of the ImageJ software (<http://rsbweb.nih.gov/ij/>). At least 5 visual fields per sample were analyzed. The experiment was performed in triplicate. For evaluation of statistical differences between control and experimental groups, we employed one-way ANOVA followed by Dunnett's test. These analyses were performed using the software Graph Path Prism 5. All values are reported as mean ± standard error (SE).

2.7.2. Nanoparticle Effects on hFOB Differentiation. The ability of hFOB 1.19 cells seeded on CNC, sCNC, oND, ND, oBINC, and BINC coated coverslips and uncoated coverslips (control group) to differentiate into mature osteoblasts was evaluated by immunofluorescent staining of the osteoblast markers: bone sialoprotein and osteocalcin. The coating of the coverslips with the different materials, cell seeding, cell incubation, fixation and permeabilization were done as explained in section 2.7.1. After permeabilization, cells were submitted to additional processing. Briefly, cell cultures were incubated with 2% normal goat serum in PBS for 1 h to block the nonspecific antibody binding. Then, they were incubated overnight in a humid chamber at 4 °C with 100 μL of a mix of the primary antibodies: mouse antiosteocalcin mAb (1:80, Abcam 13418) and rabbit antibone sialoprotein pAb (1:100, Abcam 52128). Then, cells were washed three times with PBS and incubated for 1 h at room temperature with a mix of the secondary antibodies: goat antimouse Cy3 (1:1000, Jackson ImmunoResearch Lab, USA) and goat antirabbit IgG Alexa Fluor 488 (1:500, Jackson ImmunoResearch Lab, USA). After washing three times with PBS, samples were mounted as explained in section 2.7.1. Finally, samples were analyzed using an A1R Ti-Eclipse confocal inverted microscope (Nikon) using the 40X/1.3 NA oil immersion objective under the same parameters for image acquisition to compare qualitatively fluorescence intensity between control and experimental groups. The excitation wavelengths for the fluorescent dyes Cy3 and Alexa Fluor 488 were 561 and 488 nm, respectively. Their emission was acquired at 570–620 nm and 500–550 nm, respectively. DAPI was excited at 405 nm and its emission was acquired at 425–475 nm. The pinhole used was 28 μm.

3. RESULTS

3.1. Materials Characterization. FTIR spectra (Figure 1) showed several bands in oND, ND, oBINC, and BINC that allow insight into their functional groups. The multistep synthesis of the composite was verified by comparing bands between the spectra of the intermediaries of the reaction. The first of these steps was the oxidation of the ND to form oND via the addition of carboxyl groups. In the case of the oND and the ND, a significant difference can be observed in the band at 1790 cm⁻¹, which is present only in oND. This band confirms the presence of carboxyl groups (C=O) on the surface of the nanodiamond given its higher wavenumber compared to other carbonyl moieties.²⁷ The band at 1633 cm⁻¹ is present in both oND and ND, which could be associated with the bending mode of the -OH group in water. The broad band at 3300 cm⁻¹ indicates both hydroxyl groups of ND and the carboxyl OH as well as the presences of small water clusters.²⁸ From this, it can be concluded that successful oxidation was achieved. The addition of carboxyl groups allows further chemical

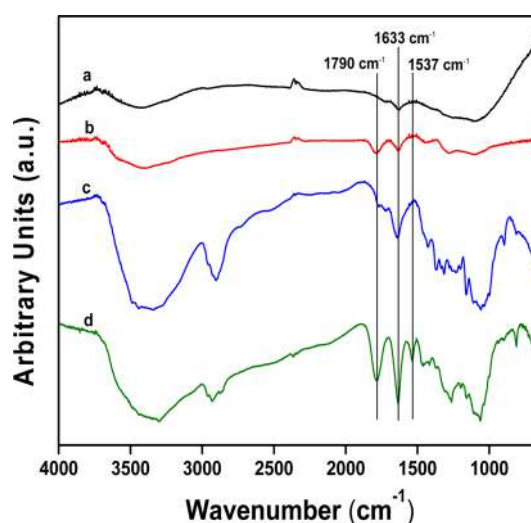


Figure 1. FTIR analysis for all ND analogues: (a) ND, (b) oND, (c) BINC, and (d) oBINC.

modification of the oND so that the other steps in the synthesis could be carried out.

Other notable bands, such as the 1790, 1640, and 1537 cm⁻¹, are sharp and well-defined in oBINC. These bands are not present or well-defined in BINC. In addition to the carbonyl band at 1790 cm⁻¹, the FTIR spectrum of the construct also shows two bands consistent with the formation of an amide bond, which proves the effectiveness of the linkage. The two bands are consistent with the well-established amide I (C=O stretching) and amide II (N-H bending) bands commonly attributed to the peptide moiety.^{27,28} Interestingly, they are only present in the final product, but noticeably absent in BINC. This absence is most likely due to the lack of sp² carboxyl carbons, which are capable of reacting with the sCNC amine to form the peptide bond. This suggests that oxidation is a necessary step in order to chemically join the diamond and cellulose. Both covalently joined products, however, have a broad band at around 3300 cm⁻¹ that does not serve as a contrast between them. Additionally, bands in the 1000–1300 cm⁻¹ range only observed in the constructs reference C-O stretching, C-H bending, and C-C stretching present in cellulose (Figure S1).²⁹

Although the presence of an amide was confirmed via FTIR analysis, the Raman spectrum allowed for the simultaneous study of cellulose nanocrystals and nanodiamonds in the product, as a means to verify if both were bound chemically or just adsorbed. The Raman spectra (Figure 2) also shows bands that allow the study of the functional groups for oND, ND, sCNC, oBINC, and BINC. All ND analogues have the same two bands around 1300 and 1600 cm⁻¹, whereas CNC lacks the presence of them. These two bands correspond to the diamond band and the G band, respectively, which are characteristic of both ND and oND, and have been well documented in the literature.³⁰ Their appearance suggests that the strong acid oxidation did not alter the integrity of the nanodiamond. However, CNC and oBINC both have a band at 2875 cm⁻¹ not present in the other samples. The cellulose band, which is observed in CNC and oBINC, proves the presence of the CNC in the final product (Figure 2). In spite of the many purification steps taken, the sCNC is still strongly bound to the oND. Most notably, it is absent in BINC. The absence of the cellulose band in BINC demonstrates the failure of the sCNC in binding to

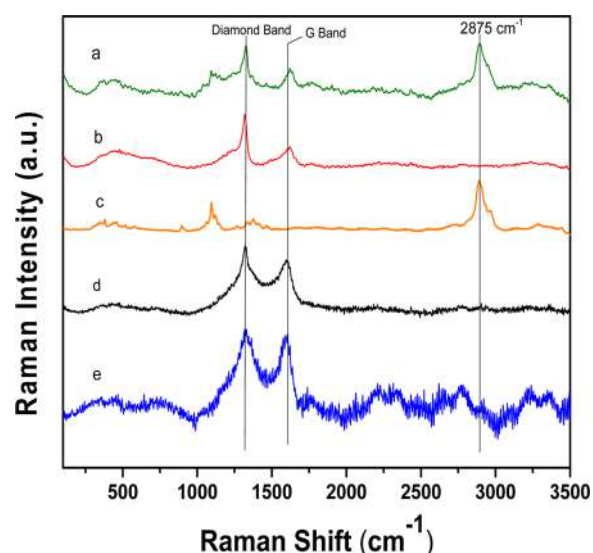


Figure 2. Raman spectra for CNC and all ND analogues (a) oBINC, (b) oND, (c) CNC, (d) ND, (e) BINC.

ND. Therefore, the binding of cellulose to diamond is likely to occur through a strong covalent bond and not just through adsorption on the surface of the diamond.

XPS analyses were completed to the CNC and ND samples. In the oBINC survey, the signals of oxygen (O 1s and O KLL), carbon (C 1s, C KLL), and silicon (Si 2s, Si 2p) can be observed. Carbon and oxygen signals are typically found in organic materials such as diamond and cellulose. APTES presence was confirmed by the Si signal (Figure 3a). Additional iron (Fe) signals were also observed due to impurities of the CNC. An XPS survey spectrum of the CNC as received is presented in Figure S1. A deconvolution of the high-resolution spectrum of the C 1s signal for oBINC sample shows four main peaks associated with 1, C–H, C–C (284.4 eV);^{31,32} 2, C–N, C–O (285.5 eV);^{32,33} 3, O–C–O (287.0 eV);³¹ 4, N–C=O (289.0 eV)³³ signals (Figure 3b). The high resolution of the carbon signal for the ND (Figure S2a) and the oND samples (Figure S2b) confirms the oxidation of the nanodiamonds after the chemical treatment. The sp^2 and sp^3 hybridizations ratios change after the chemical oxidation and additional bonds between carbon and oxygen appears at higher binding energies.

3.2. Surface Area Analysis. The analysis revealed an increase in the surface areas of the two starting materials (CNC and ND) and the final covalently linked product. The CNC showed to have a small surface area of $2.4 \text{ m}^2 \text{ g}^{-1}$, which did not change much even after silylation to $1.9 \text{ m}^2 \text{ g}^{-1}$. The ND had a surface area of $214 \text{ m}^2 \text{ g}^{-1}$. Once oxidized to oND, however, there was a 12% increase in surface area to $243 \text{ m}^2 \text{ g}^{-1}$. The area of oBINC, $244 \text{ m}^2 \text{ g}^{-1}$, remained essentially unaltered through the EDC reaction when compared to oND.

3.3. Thermal Stability Analysis. Having established the chemical union of the product, the surface area and thermal stability studies of oBINC give insight into its possible use as a biointerface material for bone cell growth. Three transitions in the TGA thermograms allow insight into the thermal stability of the ND analogues (Figure 4). The first of these transitions that occurred around $100 \text{ }^\circ\text{C}$ represents thermal dehydration and can be seen in all products. The second transition at $300 \text{ }^\circ\text{C}$ occurred on CNC and the CNCs_i-containing products. However, although the CNC and sCNC pyrolysis occurs at 300 and $250 \text{ }^\circ\text{C}$, respectively, the addition of the ND introduces

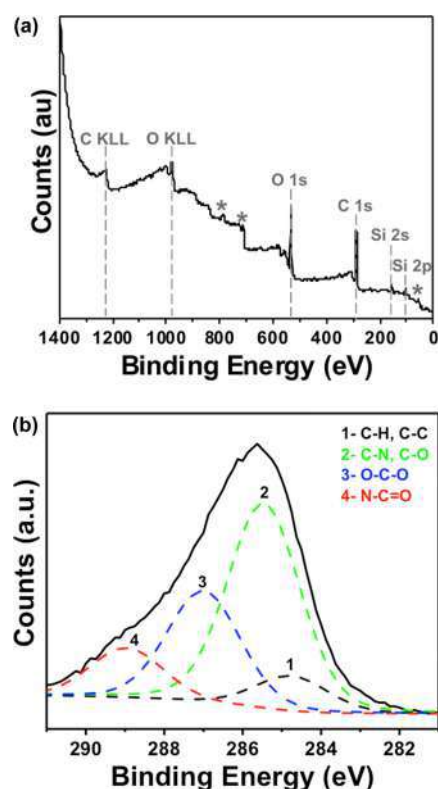


Figure 3. XPS analysis of oBINC. (a) Survey of oBINC. (b) Deconvolution of carbon signal of oBINC [1, C–H, C–C; 2, C–N, C–O; 3, O–C–O; 4, N–C=O], where * represents the Fe impurities within the CNC.

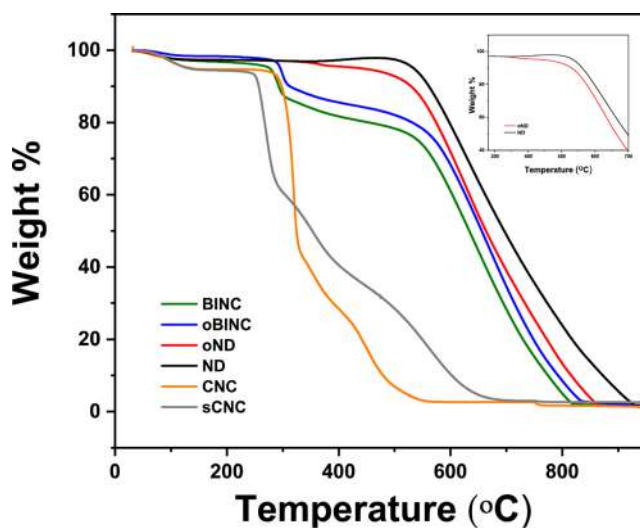


Figure 4. TGA thermograms for all ND analogues from 30 to $900 \text{ }^\circ\text{C}$ in air atmosphere.

covalent interactions that increase its thermal stability. Also, transformation of ND surface sp^2 carbons to oxygen containing groups caused by thermal oxidation generated an increase in weight % from 400 to $580 \text{ }^\circ\text{C}$ (Figure 4).³⁴ Additionally, ND showed a higher thermal stability when compared to the oND. Such a decrease in thermal stability after oxidation hints the removal of burnoff reducing surface sp^2 carbons in the acid-treated nanodiamonds. Contrariwise, the conjugate containing the oND proved to be slightly more stable than the conjugate

with ND because of additional covalent bonding between the oND carboxyl groups and the sCNC amine. The transition at 500 °C in all ND containing products represents final diamond degradation.

In addition, the surface area analysis indicates that the strong acid oxidation increased the surface area of ND by almost 12%. This increase can be attributed to the breakage of the ND during the process of oxidation. The EDC reaction, however, did not alter the surface area of ND and oND. These two parallel analyses showed that oBINC does have a high surface area and does not decompose at temperatures normally found in the human body. Its thermal stability and high surface area should prove to be desirable for human use, given that they should allow for a greater interface between implant and bone.

3.4. Zeta Potential and Dynamic Light Scattering Analysis. Zeta Potential analysis of oBINC was done in order to determine the surface charge using Malvern ZetaSizer Nano Series with 4 mV 632.8 nm laser. The suspensions were diluted with solutions at pH 3, 5, 7, 9, 11, and 13 in order to determine the Z-value at different pH. Then, 1 mL of the suspension was added to a disposable plastic cuvette, which proceeded to be analyzed. A Z-average vs pH graph (Figure 5) was plotted and

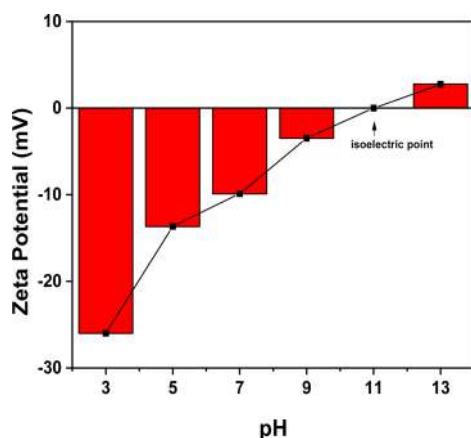


Figure 5. Variation in zeta potential with pH of oBINC.

studied to identify the isoelectric point of the conjugate. Also, the Malvern ZetaSizer was used to determine particle size distribution of ND and oND in EtOH 70%, solvent later used in biocompatibility studies (data shown in Figure S3).

3.5. Biocompatibility Studies. As an initial approach, we took optical and confocal images of hFOB 1.19 cells on ND and oND substrates, which demonstrated the noncytotoxicity of these materials and led to further biocompatibility assays (Figure S4, Figure S5). We evaluated the performance of the covalently linked cellulose nanocrystals and nanodiamonds (oBINC and BINC) as cell culture substrates for hFOB 1.19 cells by immunocytochemical analyses. We also evaluated the cell response to each one of the materials used to obtain the covalently linked nanoparticles: CNC, sCNC, oND, and ND. Cells seeded on uncoated glass coverslips were used as control groups. First, we determined the morphology that osteoblast displayed after 7 days of growth on all the materials mentioned above by labeling the actin cytoskeleton with Phalloidin-FITC (Figure 6). No morphological differences were observed between cells grown on all the surfaces. Nevertheless, cells showed to be mainly elongated and polygonal, although few spherical cells were also observed on all the surfaces. These

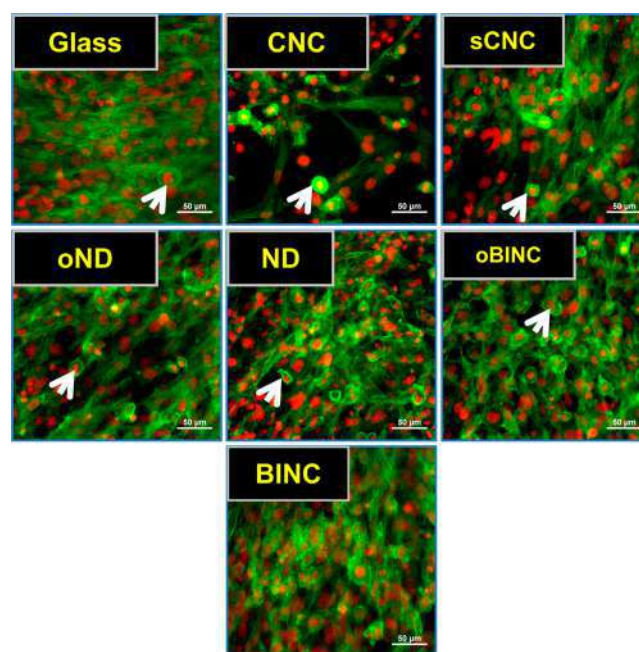


Figure 6. Nanomaterial effects on hFOB morphology. Representative images showing hFOB morphology after 7 days of culture on CNC, sCNC, oND, ND, oBINC, and BINC substrates. Cells seeded on uncoated glass coverslips are presented as controls. Actin cytoskeleton was labeled using Phalloidin-FITC (green) and cell nuclei with DAPI (blue). Most cells exhibited a fusiform or polygonal shape although some spherical cells (white arrows) were also observed. Scale bar = 50 μm .

cells were more frequently observed on oBINC and BINC surfaces. However, statistical differences were only observed when comparing glass and BINC (data shown on Figure S6). We also found that hFOB 1.19 cells formed confluent multilayers on all nanomaterials but not in CNC samples (Figure 6).

We counted the number of cells per visual field as an indicator of the degree of cell adhesion. Specifically, we determined the number of cell nuclei (labeled with DAPI) per visual field. We found that a lesser number of cells were attached on CNC ($p < 0.001$) and oBINC ($p < 0.05$) compared to uncoated glass coverslips (Figure 7A). Interestingly, osteoblasts did not grow evenly nor distributed themselves on the CNC surfaces, but instead formed cell aggregates (Figure 7B, white arrows). In general, all the materials tested allowed osteoblast cell adhesion. However, CNC and oBINC did not allow cell growth in the same manner as glass. Additionally, cells displayed a normal morphology on all the surfaces indicating no cytotoxic effects of the materials after 7 days of culture (Figure 6).

To test whether CNC, sCNC, oND, ND, oBINC, and BINC substrates support hFOB 1.19 cells differentiation, we evaluated by immunostaining the expression of bone sialoprotein and osteocalcin in hFOB cells cultured for 7 days on the materials mentioned above. Bone sialoprotein and osteocalcin are known markers of osteoblasts differentiation.³⁵ Cells cultured on uncoated glass were used as control group. Confocal imaging showed that hFOB 1.19 cells seeded on CNC, sCNC, oBINC, and BINC surfaces express bone sialoprotein (green) and osteocalcin (red) in a similar manner as cells grown on glass (Figure 8). However, lower expression levels of bone sialoprotein and osteocalcin were observed in oND and ND

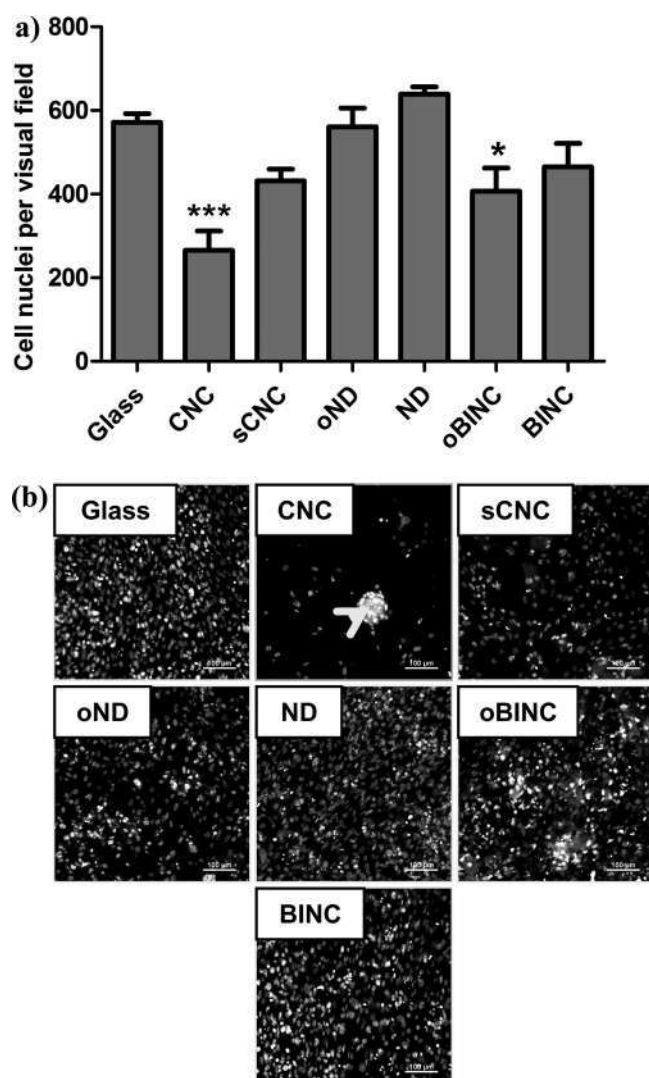


Figure 7. Nanomaterial effects on hFOB cell adhesion. (a) Each bar represents the mean hFOB nuclei \pm SE counted in at least five visual fields 20 \times per sample after 7 days of culture on each substrate. The experiment was performed in triplicate. One-way ANOVA and Dunnett' test was used for statistical analysis. *** $p < 0.001$; * $p < 0.05$. (b) Representative images showing the nuclei of hFOB cells labeled with DAPI after 7 days of culture on CNC, sCNC, oND, ND, oBINC, and BINC substrates. Cell nuclei of cells grown on glass coverslips were used as control. Cell nuclei aggregates were observed on CNC (white arrow). Scale bar = 100 μ m.

surfaces compared to control (Figure 8). Altogether, these results suggest that oND and ND do not affect the cell growth and in combination with sCNC, they appear to promote bone sialoprotein and osteocalcin expression (Figures 6 and 7).

4. DISCUSSION

Nanodiamonds (ND) prepared by detonation synthesis usually range from 2 to 10 nm in size (Figure S7), with oxygen containing groups as the most abundant of the functional groups covering its surface.³⁶ Although various surface functional groups present on commercial ND can be used for covalent functionalization, it is more convenient to homogenize the nanodiamond surface by oxidative methods. This process removes graphitic materials, followed by surface covering with carboxyl groups.³⁷ The rich chemistry of carboxyl groups

(–COOH) offers potential interactions with cellulose nanocrystals, which is one of the most promising renewable biomaterials to date. These polysaccharide nanocrystals are present in a wide variety of natural organisms and emerge as a sustainable raw material for potential applications in the biomedical field. This is due to its low cost and its outstanding mechanical properties and biocompatibility, which also shows good rates of cell attachment and proliferation.³⁸ Therefore, cellulose-nanodiamond conjugates could potentially be tailored as cell culture substrate, based on the synergistic effect that arise from the natural and physicochemical functionalities of both ND and CNC.

In an effort to develop a multifunctional biointerface material for osteoblast adhesion, proliferation and differentiation, we performed a novel construction design using ND and CNC that does not cause deleterious effects on surrounding cells and tissues. The main observation of the present work is with regards to the effects of ND on osteoblast cells. Our work has shown that human fetal osteoblastic (hFOB 1.19) cells proliferate and differentiate when cultured either on oND or ND substrates.

The in vitro experiments conducted in this study allow for a better understanding of the interaction between cells and nanostructured materials, plus show its effect on cell morphology. Previous and recent studies report that rough surfaces provide a suitable micro/nanotopography, which may significantly improve cell adhesion while also increase osteoblastic differentiation and bone formation. Results presented in this study have shown that hFOB 1.19 cells adhere on each one of the nanomaterials involved in the process to obtain the covalently joined nanodiamond-cellulose nanocrystals composites. For instance, osteoblasts show a tendency to increase their affinity and adherence for the ND. However, such affinity does not attain a statistical significance with respect to the uncoated glass substrate (control). Immunocytochemical analysis also shows no morphological differences of hFOB 1.19 cells grown on all the surfaces since cells shape looks mainly elongated and polygonal. These results could indicate that our composite and the other nanomaterials mimic, in some ways, the characteristics of the extracellular matrix and induce healthy growth of cells; suggesting no cytotoxic effects after 7 days of culture. Additionally, this analysis can be supported by the formation of confluent osteoblasts multilayers and the expression of bone matrix proteins.

When hFOB 1.19 cells differentiate into mature osteoblasts in vitro,³⁹ they express a series of proteins (e.g., bone sialoprotein, osteocalcin and collagen type I) that are involved in the process of extracellular matrix mineralization.⁴⁰ The confocal images presented in Figure 8 show that hFOB 1.19 cells seeded on a diamond-containing composite express bone sialoprotein and osteocalcin in a similar manner to the cells grown on glass. Altogether, our results suggest that nanodiamond-containing composites do not affect the cell growth, yet after oND and ND were covalently joined with sCNC, the resulting compound appears to promote and enhance the expression of bone sialoprotein and osteocalcin proteins. This could be explained, in part, due to the hydrophilic oxygen-containing surface groups of detonation ND, which easily absorbs polar molecules by hydrogen bonding as well as proteins present on the culture medium.³⁶ We therefore speculate that despite the tendency of ND to form large agglomerates, they remain at the nanoscale (around 100 nm)

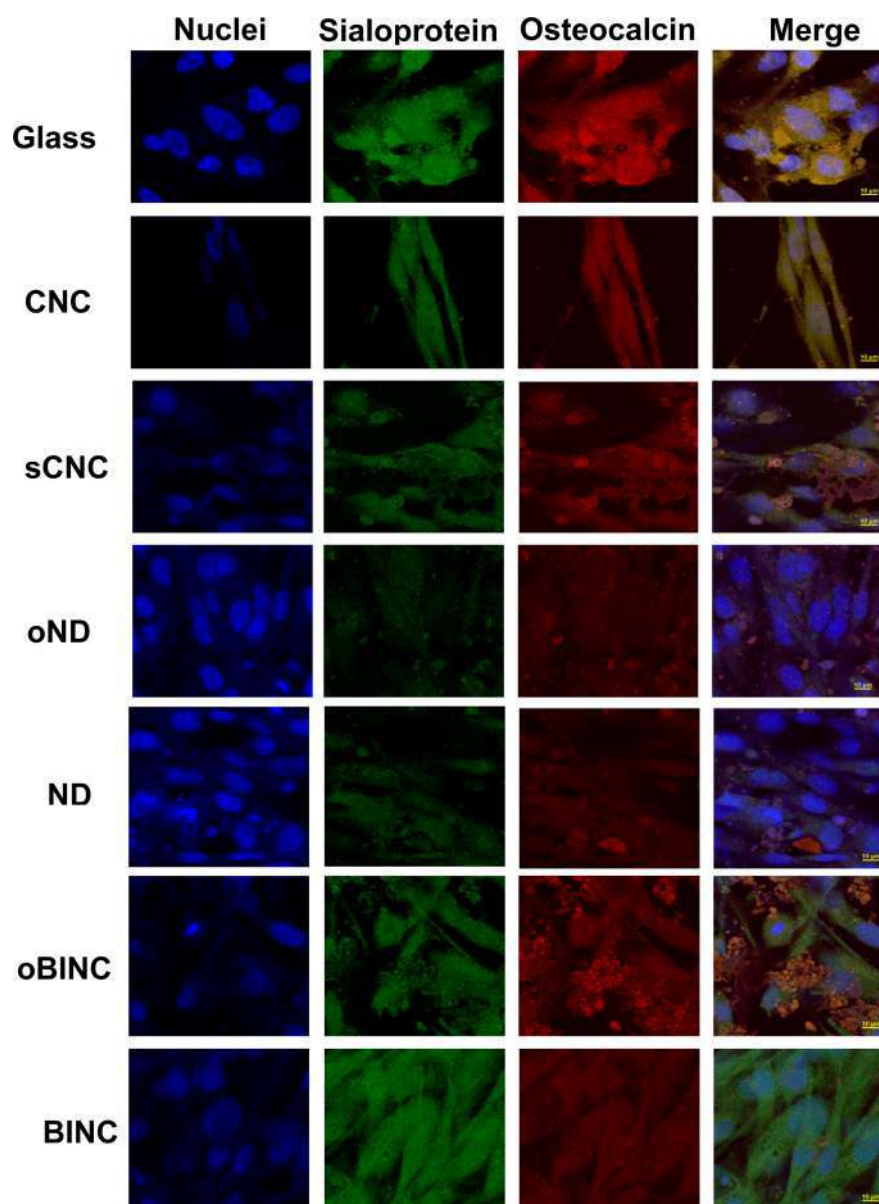


Figure 8. Nanomaterial effects on hFOB cell differentiation. Representative confocal microscopy images showing the expression of bone sialoprotein (green) and osteocalcin (red) in hFOB cells cultured for 7 days on CNC, sCNC, oND, ND, oBINC, and BINC substrates. Cells grown on glass coverslips were used as control. Cell nuclei (blue) and merged images are also displayed. Scale bar = 10 μm .

and are large enough to provide a convenient surface for osteoblast adhesion, an important previous step to accomplish differentiation. Finally, the ability to promote cell adhesion while enabling cell differentiation, simultaneously, would make oBINC well-suited to use as a potential multifunctional biointerface material.

5. CONCLUSIONS

In this work, we have demonstrated the synthesis and characterization of a biointerface material suitable for cell–biomaterial interactions, which incorporate novel nanomaterials based on detonation nanodiamonds and cellulose nanocrystals. The biological and physicochemical properties of oND have been enhanced through its covalent bonding with sCNC; demonstrating better hFOB 1.19 cell attachment, proliferation, and differentiation than the precursors materials. Moreover, the proposed and developed nanocomposite allows for a renewed

exploration of materials that could promote osseointegration. Likewise, it could serve as a biointerface material that may well allow for a better understanding of the interactions between bone implants and cells within a controlled manner for further studies. Therefore, in future works, we will evaluate oBINC and BINC capabilities as a coating for bone implants.

■ ASSOCIATED CONTENT

Supporting Information

The Supporting Information is available free of charge on the ACS Publications website at DOI: [10.1021/acsbomaterials.7b00026](https://doi.org/10.1021/acsbomaterials.7b00026).

IXPS analysis of the construct's precursor material to further support the covalent binding of CNC and ND; size distribution via dynamic light scattering and X-ray diffraction patterns of ND to provide insight on ND characteristics; quantitative and qualitative analyses of

cell proliferation on nanodiamond covered surfaces by means of a one-way ANOVA test, phase contrast microscopy, and confocal imaging (PDF)

AUTHOR INFORMATION

Corresponding Author

*E-mail: eduardo.nicolau@upr.edu.

ORCID

Eduardo Nicolau: [0000-0002-6116-029X](https://orcid.org/0000-0002-6116-029X)

Author Contributions

†K.V.-F., J.S., and C.G. contributed equally to this work. All authors have given approval to the final version of the manuscript.

Funding

This work was supported in part by the NASA Experimental Program to Stimulate Competitive Research (EPSCoR) under grant NNX14AN18A. The Neuroimaging and Electrophysiology Facility Grant NIH P20GM103642, Research Initiative for Scientific Enhancement (RISE) Program Grant 5R25GM061151-15, and the PR NASA Space Grant NNX15AI11H.

Notes

The authors declare no competing financial interest.

ACKNOWLEDGMENTS

The authors are grateful for the assistance of the UPR Material Characterization Center (MCC) and to the UPR Molecular Science Research Center for access to several resources. This work was also possible thanks to the support from The Neuroimaging and Electrophysiology Facility Grant NIH P20GM103642, Research Initiative for Scientific Enhancement (RISE) Program Grant 5R25GM061151-15, and the PR NASA Space Grant NNX15AI11H. This work was supported in part by the NASA Experimental Program to Stimulate Competitive Research (EPSCoR) Grant NNX14AN18A. We are very grateful to Dr. José E. García-Arrarás of the University of Puerto Rico, Río Piedras campus, for allowing the use of the Fluorescence Microscope obtained under Grant NSF IOS-1252679.

REFERENCES

- (1) Goldman, M.; Juodzbaly, G.; Vilkinis, V. Titanium surfaces with nanostructures influence on osteoblasts proliferation: a systematic review. *Journal of oral & maxillofacial research* **2014**, *5* (3), e1.
- (2) Loh, Q. L.; Choong, C. Three-dimensional scaffolds for tissue engineering applications: role of porosity and pore size. *Tissue Eng., Part B* **2013**, *19* (6), 485–502.
- (3) Arima, Y.; Iwata, H. Effects of surface functional groups on protein adsorption and subsequent cell adhesion using self-assembled monolayers. *J. Mater. Chem.* **2007**, *17* (38), 4079.
- (4) Wang, Q.; Yan, J.; Yang, J.; Li, B. Nanomaterials promise better bone repair. *Mater. Today* **2016**, *19*, 451.
- (5) Mazaheri, M.; Eslahi, N.; Ordikhani, F.; Tamjid, E.; Simchi, A. Nanomedicine applications in orthopedic medicine: state of the art. *Int. J. Nanomed.* **2015**, *10*, 6039–53.
- (6) Gong, T.; Xie, J.; Liao, J.; Zhang, T.; Lin, S.; Lin, Y. Nanomaterials and bone regeneration. *Bone Res.* **2015**, *3*, 15029.
- (7) McMahon, R. E.; Wang, L.; Skoracki, R.; Mathur, A. B. Development of nanomaterials for bone repair and regeneration. *J. Biomed. Mater. Res., Part B* **2013**, *101* (2), 387–397.
- (8) Peng, H.; Liu, X.; Wang, R.; Jia, F.; Dong, L.; Wang, Q. Emerging nanostructured materials for musculoskeletal tissue engineering. *J. Mater. Chem. B* **2014**, *2* (38), 6435–6461.

- (9) Tang, Z.; He, C.; Tian, H.; Ding, J.; Hsiao, B. S.; Chu, B.; Chen, X. Polymeric nanostructured materials for biomedical applications. *Prog. Polym. Sci.* **2016**, *60*, 86–128.

- (10) Kossovsky, N.; Gelman, A.; Hnatyszyn, H. J.; Rajguru, S.; Garrell, R. L.; Torbati, S.; Freitas, S. S. F.; Chow, G.-M. Surface-Modified Diamond Nanoparticles as Antigen Delivery Vehicles. *Bioconjugate Chem.* **1995**, *6* (5), 507–511.

- (11) Schrand, A. M.; Huang, H.; Carlson, C.; Schlager, J. J.; Osawa, E.; Hussain, S. M.; Dai, L. Are diamond nanoparticles cytotoxic? *J. Phys. Chem. B* **2007**, *111* (1), 2–7.

- (12) Thomas, V.; Halloran, B. A.; Ambalavanan, N.; Catledge, S. A.; Vohra, Y. K. In vitro studies on the effect of particle size on macrophage responses to nanodiamond wear debris. *Acta Biomater.* **2012**, *8* (5), 1939–47.

- (13) Puzyr, A. P.; Tarskikh, S. V.; Makarskaya, G. V.; Chiganova, G. A.; Larionova, I. S.; Detkov, P. Y.; Bondar, V. S. Damaging Effect of Detonation Diamonds on Human White and Red Blood Cells in vitro. *Dokl. Biochem. Biophys.* **2002**, *385* (1/6), 201–204.

- (14) Garcia, Y.; Ruiz-Blanco, Y. B.; Marrero-Ponce, Y.; Sotomayor-Torres, C. M. Orthotropic Piezoelectricity in 2D Nanocellulose. *Sci. Rep.* **2016**, *6*, 34616.

- (15) Ribeiro, C.; Sencadas, V.; Correia, D. M.; Lanceros-Mendez, S. Piezoelectric polymers as biomaterials for tissue engineering applications. *Colloids Surf., B* **2015**, *136*, 46–55.

- (16) Ribeiro, C.; Moreira, S.; Correia, V.; Sencadas, V.; Rocha, J. G.; Gama, F. M.; Gómez Ribelles, J. L.; Lanceros-Méndez, S. Enhanced proliferation of pre-osteoblastic cells by dynamic piezoelectric stimulation. *RSC Adv.* **2012**, *2* (30), 11504.

- (17) Ribeiro, C.; Correia, V.; Martins, P.; Gama, F. M.; Lanceros-Mendez, S. Proving the suitability of magnetoelectric stimuli for tissue engineering applications. *Colloids Surf., B* **2016**, *140*, 430–6.

- (18) Tashiro, K.; Kobayashi, M. Theoretical evaluation of three-dimensional elastic constants of native and regenerated celluloses: role of hydrogen bonds. *Polymer* **1991**, *32* (8), 1516–1526.

- (19) Hsu, M. H.; Chuang, H.; Cheng, F. Y.; Huang, Y. P.; Han, C. C.; Chen, J. Y.; Huang, S. C.; Chen, J. K.; Wu, D. S.; Chu, H. L.; Chang, C. C. Directly thiolated modification onto the surface of detonation nanodiamonds. *ACS Appl. Mater. Interfaces* **2014**, *6* (10), 7198–203.

- (20) Dhanak, V. R.; Butenko, Y. V.; Brieva, A. C.; Coxon, P. R.; Alves, L.; Šiller, L. Chemical Functionalization of Nanodiamond by Amino Groups: An X-Ray Photoelectron Spectroscopy Study. *J. Nanosci. Nanotechnol.* **2012**, *12* (4), 3084–3090.

- (21) Lee, G.-J.; Kim, C. K.; Bae, Y.; Rhee, C. K. Surface Modification to Improve Hydrophobicity of Detonation Nanodiamond. *J. Nanosci. Nanotechnol.* **2012**, *12* (7), 5995–5999.

- (22) Taglietti, A.; Arciola, C. R.; D'Agostino, A.; Dacarro, G.; Montanaro, L.; Campoccia, D.; Cucca, L.; Vercellino, M.; Poggi, A.; Pallavicini, P.; Visai, L. Antibiofilm activity of a monolayer of silver nanoparticles anchored to an amino-silanized glass surface. *Biomaterials* **2014**, *35* (6), 1779–88.

- (23) Nicolau, E.; Mendez, J.; Fonseca, J. J.; Griebenow, K.; Cabrera, C. R. Bioelectrochemistry of non-covalent immobilized alcohol dehydrogenase on oxidized diamond nanoparticles. *Bioelectrochemistry* **2012**, *85*, 1–6.

- (24) Shin, Y.-R.; Jung, S.-M.; Jeon, I.-Y.; Baek, J.-B. The oxidation mechanism of highly ordered pyrolytic graphite in a nitric acid/sulfuric acid mixture. *Carbon* **2013**, *52*, 493–498.

- (25) Powell, H. M.; Boyce, S. T. EDC cross-linking improves skin substitute strength and stability. *Biomaterials* **2006**, *27* (34), 5821–7.

- (26) Bartczak, D.; Kanaras, A. G. Preparation of peptide-functionalized gold nanoparticles using one pot EDC/sulfo-NHS coupling. *Langmuir* **2011**, *27* (16), 10119–23.

- (27) Varley, T. S.; Hirani, M.; Harrison, G.; Holt, K. B. Nanodiamond surface redox chemistry: influence of physicochemical properties on catalytic processes. *Faraday Discuss.* **2014**, *172*, 349–64.

- (28) Wolcott, A.; Schiros, T.; Trusheim, M. E.; Chen, E. H.; Nordlund, D.; Diaz, R. E.; Gaathon, O.; Englund, D.; Owen, J. S. Surface Structure of Aerobically Oxidized Diamond Nanocrystals. *J. Phys. Chem. C* **2014**, *118* (46), 26695–26702.

(29) Mazurek, S.; Mucciolo, A.; Humbel, B. M.; Nawrath, C. Transmission Fourier transform infrared microspectroscopy allows simultaneous assessment of cutin and cell-wall polysaccharides of Arabidopsis petals. *Plant J.* **2013**, *74* (5), 880–91.

(30) Osswald, S.; Yushin, G.; Mochalin, V.; Kucheyev, S. O.; Gogotsi, Y. Control of sp²/sp³ carbon ratio and surface chemistry of nanodiamond powders by selective oxidation in air. *J. Am. Chem. Soc.* **2006**, *128* (35), 11635–42.

(31) Zhang, J.; Zhang, J.; Lin, L.; Chen, T.; Zhang, J.; Liu, S.; Li, Z.; Ouyang, P. Dissolution of microcrystalline cellulose in phosphoric acid—molecular changes and kinetics. *Molecules* **2009**, *14* (12), 5027–41.

(32) Barazzouk, S.; Daneault, C. Amino Acid and Peptide Immobilization on Oxidized Nanocellulose: Spectroscopic Characterization. *Nanomaterials* **2012**, *2* (4), 187–205.

(33) Melnik, E.; Muellner, P.; Bethge, O.; Bertagnolli, E.; Hainberger, R.; Laemmerhofer, M. Streptavidin binding as a model to characterize thiol-ene chemistry-based polyamine surfaces for reversible photonic protein biosensing. *Chem. Commun.* **2014**, *50* (19), 2424–7.

(34) Huang, H.; Dai, L.; Wang, D. H.; Tan, L.-S.; Osawa, E. Large-scale self-assembly of dispersed nanodiamonds. *J. Mater. Chem.* **2008**, *18* (12), 1347.

(35) Marom, R.; Shur, I.; Solomon, R.; Benayahu, D. Characterization of adhesion and differentiation markers of osteogenic marrow stromal cells. *J. Cell. Physiol.* **2005**, *202* (1), 41–8.

(36) Krueger, A. The structure and reactivity of nanoscale diamond. *J. Mater. Chem.* **2008**, *18* (13), 1485.

(37) Mochalin, V. N.; Shenderova, O.; Ho, D.; Gogotsi, Y. The properties and applications of nanodiamonds. *Nat. Nanotechnol.* **2012**, *7* (1), 11–23.

(38) Granja, P. L.; Jéso, B. D.; Bareille, R.; Rouais, F.; Baquey, C.; Barbosa, M. A. Cellulose phosphates as biomaterials. In vitro biocompatibility studies. *React. Funct. Polym.* **2006**, *66* (7), 728–739.

(39) Yen, M. L.; Chien, C. C.; Chiu, I. M.; Huang, H. I.; Chen, Y. C.; Hu, H. I.; Yen, B. L. Multilineage differentiation and characterization of the human fetal osteoblastic 1.19 cell line: a possible in vitro model of human mesenchymal progenitors. *Stem Cells* **2007**, *25* (1), 125–31.

(40) Harris, S. A.; Enger, R. J.; Riggs, B. L.; Spelsberg, T. C. Development and characterization of a conditionally immortalized human fetal osteoblastic cell line. *J. Bone Miner. Res.* **1995**, *10* (2), 178–86.

■ NOTE ADDED AFTER ASAP PUBLICATION

There was an error in Figure 3b in the version published ASAP April 13, 2017; the corrected version was published ASAP April 14, 2017.